agronomy

MDPI

Article

Interval-Dependent Discrimination of Mineral Nutrient Supply Levels by Leaf Electrical and SPAD Measurements in Winter Wheat: A Paired Internal Benchmark Study

Shuang Zhang [1,2], Bo Zhang [2,*], Xintong Du [2], Xinkang Hu [1,3] and Chundu Wu [1,2,4,5,*]

1 School of Agricultural Engineering, Jiangsu University, Zhenjiang 212013, China; shua.zhang@stmail.ujs.edu.cn (S.Z.); huxinkang@jsafc.edu.cn (X.H.)
2 School of Environment and Safety Engineering, Jiangsu University, Zhenjiang 212013, China
3 School of Mechanical and Electrical Engineering, Jiangsu Vocational College of Agriculture and Forestry, Zhenjiang 212400, China
4 Key Laboratory for Theory and Technology of Intelligent Agricultural Machinery and Equipment, Jiangsu University, Zhenjiang 212013, China
5 Jiangsu Province and Education Ministry Cosponsored Synergistic Innovation Centre of Modern Agricultural Equipment, Jiangsu University, Zhenjiang 212013, China
* Correspondence: zhangbo@ujs.edu.cn (B.Z.); wucd@ujs.edu.cn (C.W.)

Abstract

Leaf-based sensors can characterize crop responses to nutrient supply, but their relative performance may differ across supply intervals. We compared five electrical descriptors extrapolated to zero clamping force with optical SPAD readings collected from the same winter-wheat vessels on the same dates. The experiment covered four compound mineral supply formulations (25%, 50%, 75%, and 100%) and three adjacent contrasts. The paired B2 dataset comprised 192 vessel–date observations from 12 vessels across 16 dates. We evaluated four feature sets using seven classifiers, with nested leave-one-date-out validation as the primary analysis and alternative leave-out schemes as sensitivity checks. In the reproductive stage, electrical resistance (IR) outperformed SPAD for the 25–50% contrast (date-averaged area under the receiver operating characteristic curve [ROC-AUC]: 0.870 versus 0.574; ΔAUC = +0.296; 95% date-cluster bootstrap interval: +0.092 to +0.491), whereas SPAD outperformed IR for the 75–100% contrast (0.981 versus 0.352; IR − SPAD ΔAUC = −0.630; interval: −0.871 to −0.352). Thus, the relative ranking reversed across the two endpoint intervals. Performance in the intermediate interval varied with feature representation and classifier, and fusion did not exceed the strongest non-fused feature set in the six reference-model tasks. Electrical-only results also differed between B1 and B2, although B1 could not test the paired optical–electrical ranking. These findings support reporting the target formulation interval, feature–classifier specification, validation design, and cross-batch evidence when comparing leaf sensors. The results concern assigned compound formulations, not calibrated plant nutrient diagnoses or management thresholds.

Keywords: wheat; electrical measurement; SPAD; compound mineral supply; interval of discriminative advantage; sensor benchmark comparison; grouped cross-validation; cross-date domain shift; sensing-modality selection

Check for updates

Academic Editor: Shri Mohan Jain

Received: 14 October 2026
Revised: 22 October 2026
Accepted: 4 November 2026
Published: 7 November 2026

Copyright: © 2026 by the authors. Licensee MDPI, Basel, Switzerland. This article is an open access article distributed under the terms and conditions of the Creative Commons Attribution (CC BY) license.

1. Introduction

Wheat is a major cereal crop underpinning global food security [1,2]. However, wheat production is increasingly challenged by climatic variability, disease pressure, and constraints on water and fertilizer resources [3]. Insufficient nutrient supply restricts leaf

expansion and photosynthetic capacity, whereas excessive fertilization reduces N-use efficiency and increases environmental burdens [4,5]. More broadly, coordinated management of water and nutrients is essential for narrowing yield gaps while improving resource-use efficiency [6–8]. Accordingly, rapid and non-destructive sensing of crop responses to nutrient supply is important for precision nutrient management.

Non-destructive, rapid leaf measurement is a core tool of plant nutrient monitoring. The SPAD reading is a dual-wavelength leaf-transmittance optical index (quantifying red and near-infrared transmission spectra at 650 and 940 nm) related to chlorophyll rather than an extractive measurement of chlorophyll content or tissue nitrogen, and its empirical calibration may be nonlinear and condition-dependent [9,10]. Tissue-electrical parameters such as resistance, impedance, capacitive reactance, inductive reactance, and capacitance are associated with cell-membrane architecture, ion concentrations, membrane-polarization capacity, tissue water content, and intercellular conductive pathways [11–15]. Electrical-impedance measurement is a non-destructive, rapid sensing technique that responds to changes in plant-tissue electrical properties associated with physiological and structural variation [16–18] and has been used for nutrition-related signal analysis and stress classification [19–24]. Because the two measurement types reflect different tissue properties, their discrimination performance should be compared within well-defined supply intervals. For practical sensing tasks, the basis for modality selection must also state the growth stage and validation conditions and cannot rest on a single global metric: repeated readings on the same vessels and dates are not independent replicates, so the comparison requires a validation scheme that respects that dependency and avoids model-selection bias [25–29].

Whole-gradient accuracy or correlation can obscure differences between adjacent supply levels when sensor response curves vary across the gradient. A paired comparison on the same vessels and dates reduces differences in sampling context between electrical and optical measurements and directly tests whether their relative discrimination changes with the target interval.

The comparison therefore targets a practical question: to tell a 25% supply from a 50% supply, which sensor should a grower use? An overall accuracy of 80% could conceal 95% accuracy for one contrast and 50% for another, and the weaker contrast may be the one that matters for a particular monitoring decision. Because a ranking metric does not specify an operational decision threshold, we evaluated discrimination using ROC-AUC rather than interpreting the results as a ready-to-use classification rule.

We compared three adjacent formulation contrasts (25–50%, 50–75%, and 75–100%) separately rather than treating the full gradient as one classification problem. The central question was whether the relative ranking of electrical and SPAD representations changes with the target contrast. These labels denote experimentally assigned compound mineral formulations, not measured tissue nutrient status or agronomic fertilizer thresholds.

The specific objectives were to (1) compare paired electrical and SPAD measurements on the same vessel–date units using nested leave-one-date-out (LODO) validation, with leave-one-vessel-identifier-out (LOVIO) and joint leave-out as internal sensitivity analyses; (2) determine whether the relative fixed-label ranking performance changes among adjacent supply intervals and among feature–classifier representations; (3) distinguish fixed-direction predictive AUC from post hoc direction-selected marginal separation; and (4) assess the electrical-only cross-batch pattern and synthesize the observed conditions into an evidence-informed reporting specification. The central empirical question is whether a favorable within-batch ranking in one formulation contrast can reasonably be treated as a general sensor advantage.

2. Materials and Methods

2.1. Plant Materials, Cultivation, Batch Timeline, and Measurement Hierarchy

Winter wheat (*Triticum aestivum* L., cultivar Yangmai 23) was grown at Jiangsu University in two temporally distinct cultivation batches (B1 and B2), hydroponically in an outdoor polyolefin (PO) film greenhouse rather than in open-field soil. Germination of B1 began on 8 October 2025, with transplanting on 18 October and the start of compound supply treatments on 23 October; the corresponding dates for B2 were 1 March, 16 March and 31 March 2026. Electrical measurements of B1 covered 3 November–22 December 2025 (vegetative) and 24 December 2025–29 January 2026 (reproductive). Those of B2 covered 6 April–20 May 2026 (vegetative, 12 dates) and 25 May–24 June 2026 (reproductive, 7 dates), 19 dates in total, of which 16 were retained in the dual-modality matched set (Section 2.5); the matched data comprise 10 vegetative and 6 reproductive dates. The two batches' observation windows do not overlap, so dates identify the batch (Table 1). The three destructive sampling dates were assigned by the same rule: 19 December 2025 and 29 January 2026 to B1, and 19 June 2026 to B2; of the 36 physicochemical samples described in Section 2.3, 24 come from B1 and 12 from B2, and all vegetative-stage samples come from B1 (Supplementary Table S5 includes a "cultivation batch" column).

Table 1. Key operational timeline and solution-renewal cycle of the two cultivation batches. B1 and B2 do not overlap in time, so measurement dates uniquely identify batch. Complete solution renewal was performed every 5 days; at each renewal, the three vessels of the same "batch × formulation" group shared one fresh preparation, and their positions were re-randomized.

Operation	Batch B1	Batch B2
Germination onset	8 October 2025	1 March 2026
Transplanting into vessels	18 October 2025	16 March 2026
Start of compound supply treatment	23 October 2025	31 March 2026
Complete solution renewal and random vessel repositioning	Every 5 d	Every 5 d

Seedlings were initially raised in 100% reference nutrient solution, and plants of uniform appearance were selected for transplanting. Each batch comprised four compound supply formulations (25%, 50%, 75%, and 100%), each assigned to three fixed cylindrical PET cultivation vessels (about 10 cm in diameter and 20 cm in height), each containing approximately 1.2 L of nutrient solution and two wheat plants, giving 24 distinct vessels across the two batches. Eligible vessels were randomly selected at the start of treatment; vessel identifiers 1–3 within each "batch × formulation" combination were assigned randomly and then held constant. Vessels were arranged in a staggered layout in the greenhouse, and their positions were re-randomized at each complete solution renewal, performed every 5 d. At each renewal, the three vessels of the same "batch × formulation" combination shared a single approximately 3.6 L preparation, subdivided into three portions of about 1.2 L; vessels are therefore replicated cultivation units but not replicates of independently prepared nutrient solution, and we account for this structure in all inference.

A 15 fil PO film (C.I. TAKIRON A 150-μm PO film (C.I. TAKIRON Corporation, Osaka, Japan; nominal thickness about 0.15 mm) covered the greenhouse, with manufacturer-stated attenuation of UV-B, transmission of UV-A, and a nominal photosynthetically active radiation transmittance of about 90–92%; waveband-specific transmittance—particularly in the blue-light region (400–500 nm), which modulates stomatal behaviour—was not spectrally measured here. The greenhouse was naturally ventilated, so small-scale microclimatic differences between edge and center positions cannot be excluded. The nutrient solution

was prepared with deionized water without active aeration, and pH, electrical conductivity and rhizosphere ion composition were not continuously monitored or adjusted.

The cultivation vessel is the longitudinally tracked unit, the "vessel × date" is the observation unit, and "batch × formulation × renewal day" is the shared solution-preparation source; a new measurement date is not a new independent treatment replicate. The two plants per vessel were not individually tracked, so all longitudinal analyses and modality matching use the vessel, not identifiable individual plants, as the unit. Because preparation events and vessel trajectories are correlated, the bootstrap intervals reported here are conditional uncertainty indicators rather than interval estimates of independent preparation-level treatment effects.

For interpretation of the effective sample size, each formulation was represented by three longitudinally followed vessels, not three independently prepared nutrient solutions; repeated readings within a vessel–date were averaged before classification, and neither dates nor vessel–date records are independent preparation replicates (Supplementary Tables S8 and S15).

2.2. Leaf Electrical Acquisition and Clamping-Force Extrapolation

Following the existing fitting and zero-force extrapolation schemes described in Zhang's doctoral dissertation [30] and Tan et al. [31], we obtained five descriptors: resistance IR, impedance IZ, capacitive reactance IXc, inductive reactance IXl, and capacitance ICP. Capacitance follows a linear force–capacitance relation and the other four follow exponential relations; the zero-force descriptors are the fitted functions evaluated at F = 0 and are not new models proposed here. Instrument channels, fitted forms, extrapolation expressions, and zero/outlier handling are given in Supplementary Table S9 and reproduced in full in Supplementary Methods S3. A HIOKI 3532-50 LCR meter (HIOKI E.E. Corporation, Ueda, Nagano, Japan) was used at 3 kHz and 1.5 V rms, with two 8 mm-diameter copper electrodes clamping the mesophyll on both sides of the leaf midrib (Figure 1). Measurements were taken between 09:00 and 11:00; the third fully expanded leaf was measured in the vegetative stage and the flag leaf in the reproductive stage. A computer-controlled device applied eight clamping-force levels from 2 to 9 N in sequence, with readings taken after 5 s of stabilization at each level [30,31].

Zero-force extrapolation was used to reduce dependence on electrode clamping force, not to show that contact effects are fully removed. Electrode placement followed the same anatomical rule as in Section 2.3 (third leaf in the vegetative stage, flag leaf in the reproductive stage), but exact placement consistency across dates was not independently audited.

This study uses these descriptors only for sensor discrimination comparison across compound mineral supply intervals, without new mechanistic derivation or independent revalidation of the force–electrical models; the reproducible inputs are the archived zero-force descriptor values, while the underlying eight-level raw force–electrical readings remain with the authors and are not part of the public supplementary archive. The dataset was cross-checked against the ideal conversion relation $IC = \frac{1}{2\pi f IX_C}$ (f = 3 kHz) for ICP and IXc: about 98% of checkable records have ratios within 1.000 ± 0.01, so the five descriptors were retained as originally archived; individual records deviate, their origin cannot be determined from the archived data, and no records were removed or corrected on this basis. Meteorological covariates recorded during electrical measurements (Section 2.9) are shared by all vessels on a date and therefore describe date-level, not vessel-level, conditions.

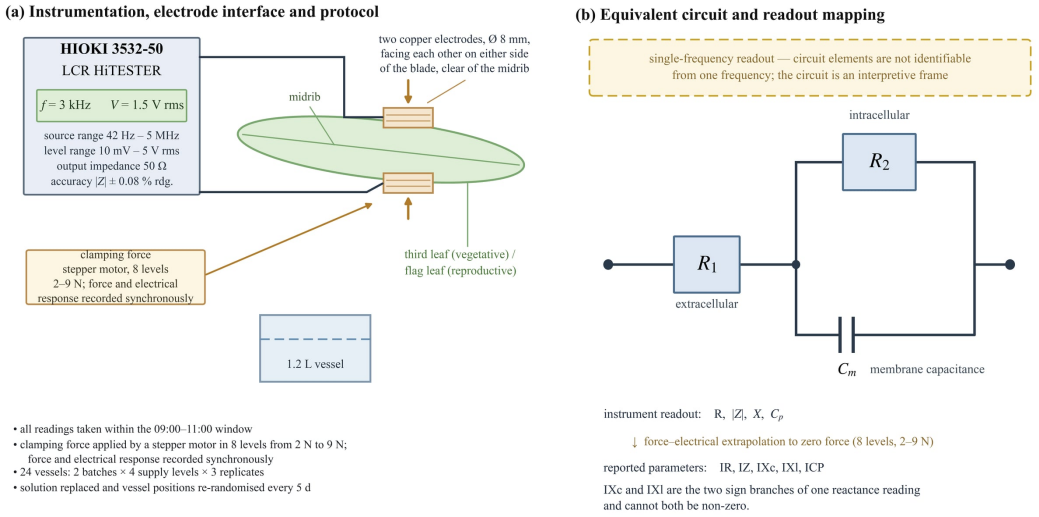


Figure 1. Leaf electrical measurement setup and conceptual readout model. (**a**) Instrumentation, electrode interface and protocol. Navy lines indicate the measurement wiring between the LCR meter and the two 8 mm copper electrodes; amber arrows indicate the clamping force applied through the electrode pair by the stepper motor; differently coloured boxes distinguish the instrument, the electrode–leaf interface and the measurement protocol. (**b**) Interpretive equivalent circuit and readout mapping: R1 is the series (extracellular) resistance, R2 the intracellular branch and Cm the membrane-associated capacitance. The circuit is an interpretive frame for the single-frequency readouts (R, |Z|, X and Cp); it is not fitted to the data, and its elements are not uniquely identifiable from one frequency.

2.3. Optical Measurements and Auxiliary Biochemical and Growth Phenotypes

In batch B2, SPAD was generally measured before electrical readings on the same leaf, within the daily 09:00–11:00 window, using a SPAD-502 Plus chlorophyll meter (Konica Minolta Sensing, Inc., Osaka, Japan); the arithmetic mean was taken as the leaf SPAD value at the upper, middle and lower positions of the sampled leaf; the arithmetic mean was taken as the leaf SPAD value. This usual order was not formally randomized or documented for every observation; no contact-related damage was visible, but transient or microscopic contact effects cannot be excluded. The two modalities were paired at the vessel–date level rather than by individually tracked plants (the cultivation and matched-measurement design and the analytical sample flow are shown in Figure 2).

The 36 destructive samples were taken from the longitudinally tracked vessels themselves (12 per sampling date: 4 supply levels × 3 vessels), and no additional vessels were established. The 12 B2 samples were taken on 19 June 2026, the last date of the B2 matched set, after which no further paired measurements were made, so the remaining 180 paired records on 15 dates are unaffected. The two B1 samplings occurred in the vegetative stage (19 December 2025, after which those vessels continued to be measured until 29 January 2026) and at the end of the reproductive stage. A slight effect of vegetative-stage sampling on subsequent readings of the same vessel cannot be excluded; those subsequent observations were therefore retained and the potential effect is listed as a limitation (Section 4.5). Because the primary paired comparison was conducted exclusively in B2, any such carry-over in B1 cannot affect the B2 paired estimates, though it remains a possible source of variation in the B1 electrical-only analyses.

These physicochemical data serve only as a traceability audit archive: they enter no discrimination model and are not a criterion of treatment effectiveness. The 36 individual observations, with the five electrical parameters measured at the same time, are listed in Supplementary Table S5 with the batch annotated row by row; assay methods appear in Supplementary Methods S1 and the empirical resolution of these data in Section 3.11.

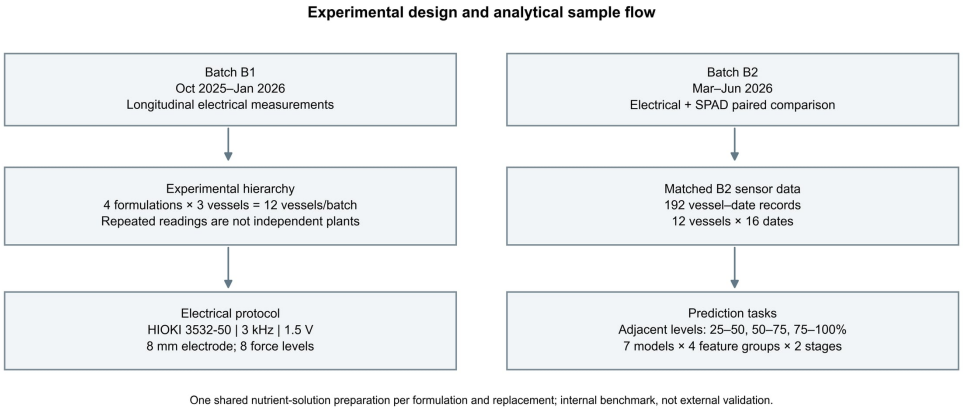


Figure 2. Cultivation batches, experimental units, and paired data flow. B1 contains only electrical records; B2 contains both electrical and SPAD records. Each batch has four supply levels with three fixed vessels per level and two plants per vessel; B2 forms 12 vessels × 16 dates = 192 matched vessel–date records, and each of three adjacent intervals is compared with seven algorithms and four feature sets. Vessels of the same treatment share solution preparation, so vessel–date records are not independent preparation replicates. The four feature sets are built from only two acquisition modalities—optical transmittance and electrical impedance—as SPAD alone, IR alone, Electrical5 and Fusion. Take-home: the paired comparison is between two modalities measured on the same leaves, while four feature representations are scored within it.

2.4. Compound Mineral Supply Formulations

The 100% reference formulation contains KNO_3 (506 mg L^{-1}), NH_4NO_3 (80 mg L^{-1}), $Ca(NO_3)_2{\cdot}4H_2O$ (945 mg L^{-1}), KH_2PO_4 (136 mg L^{-1}), $MgSO_4$ (241 mg L^{-1}), FeNaEDTA (36.7 mg L^{-1}), KI (0.83 mg L^{-1}), H_3BO_3 (6.2 mg L^{-1}), $MnSO_4$ (22.3 mg L^{-1}), $ZnSO_4$ (8.6 mg L^{-1}), Na_2MoO_4 (0.25 mg L^{-1}), $CuSO_4$ (0.025 mg L^{-1}), and $CoCl_2$ (0.025 mg L^{-1}) [32]. The 25%, 50%, and 75% nominal treatments scale down only KNO_3, NH_4NO_3, and $Ca(NO_3)_2{\cdot}4H_2O$ proportionally, with all other listed salts unchanged; no nitrogen-free potassium or calcium salts were added to balance K or Ca. The treatment labels therefore denote the proportional scaling of three selected salts rather than equal proportional changes in total N, K, Ca, or all mineral elements. NH_4NO_3 supplies both ammonium and nitrate nitrogen (Table 2).

Table 2. Theoretical total supply concentrations (mmol L^{-1}) of the four compound mineral formulations calculated from nominal salt additions. KNO_3, NH_4NO_3, and $Ca(NO_3)_2{\cdot}4H_2O$ are scaled proportionally to the treatment level, while KH_2PO_4, $MgSO_4$, and the listed micronutrient salts are held constant. Nominal supplies of N, K, and Ca therefore co-vary; Ca/N is about 0.267, whereas K/N decreases from about 0.600 at the 25% level to about 0.400 at the 100% level. Values are theoretical formulation values, not measured solution element concentrations, EC, or pH, and cannot be used to identify nitrogen-specific effects.

Nominal Formulation	Total N (mmol L^{-1})	Total K (mmol L^{-1})	Total Ca (mmol L^{-1})	K/N	Ca/N
25%	3.75	2.25	1.00	0.600	0.267
50%	7.50	3.50	2.00	0.467	0.267
75%	11.26	4.75	3.00	0.422	0.266
100%	15.01	6.00	4.00	0.400	0.266

After preparation, we checked the solution pH and electrical conductivity (EC) with a Lichenwith a Lichen PH-100 pH meter and a Lichen CT-20 conductivity meter (Shanghai Lichen-BX Instrument Technology Co., Ltd., Shanghai, China), respectively. The reference guidance for the 100% standard formulation was approximately 2 mS cm^{-1} for EC and

pH 5.5–7.5; these reference values must not be interpreted as measured values for all four formulations. The checks were operational rather than systematically recorded experimental variables, and no acid or base was added to adjust pH. Individual readings were not retained, so treatment-specific pH/EC differences and temporal changes in solution chemistry cannot be quantified retrospectively.

2.5. Data Preprocessing and Analytical Samples

Repeated electrical records sharing batch, growth stage, date, supply level and fixed vessel identifier were averaged into a single vessel–date observation, yielding 814 aggregated records over 71 measurement dates (52 in B1, 19 in B2) and 275 date–level cells; the raw electrical audit comprised 831 records, of which 17 excess same-vessel-same-day records were aggregated, and nine of the 284 potential date–level cells lacked complete electrical records for that level. The optical–electrical matched set contains 192 records (12 vessels × 16 dates in B2), and modality comparisons use only this matched set; B1 electrical records serve two batch-pooled auxiliary analyses—within-group dispersion and meteorological predictive skill—and the cross-batch test of Section 3.10. Each adjacent-level task has 10 dates and 60 matched observations in the vegetative stage and 6 dates and 36 observations in the reproductive stage. Counts and their reconciliation are given in Supplementary Tables S8, S15 and S16, with the full accounting in Supplementary Results S17.

B2 yielded electrical records on 19 measurement dates, of which 16 had complete electrical records at all four supply levels together with synchronous SPAD; the other three were excluded for incomplete level coverage (13 and 28 April 2026 each carried only the 100% level; 24 June 2026 lacked it). We applied a common complete-date criterion so that all three adjacent intervals rest on the same 16 dates rather than on interval-specific subsets. It was applied according to measurement availability, irrespective of the observed values, but this does not establish that the missingness mechanism was independent of the unobserved measurements, so the estimates remain conditional on those 16 dates.

2.6. Within-Group Variation

For each growth stage, date, supply level and descriptor, we computed between-vessel dispersion on the natural-log scale and expressed it as a ratio R against the pooled within-cell reference; the definition, the estimator and its bootstrap are given in Supplementary Methods S4.

2.7. Date-Matched Discrimination and Nested Temporal Group Validation

Adjacent compound supply levels (25–50%, 50–75%, and 75–100%) were compared separately within each growth stage using the common set of 16 B2 measurement dates with complete electrical and SPAD records at all four formulation levels, as defined in Section 2.5. Each vegetative-stage task contained 10 dates and 60 vessel–date records (three vessels per formulation level per date), whereas each reproductive-stage task contained six dates and 36 records. Seven classification algorithms (logistic regression, linear SVM, RBF-kernel SVM, random forest, extra trees, KNN, and histogram-based gradient boosting) were crossed with four feature sets—SPAD alone; IR alone; Electrical5, a feature set formed by the juxtaposition of IR, IZ, IXc, IXl and ICP; and Fusion, SPAD concatenated with Electrical5—forming a 7 algorithms × 4 feature sets × 3 intervals × 2 stages design. The main comparison uses leave-one-date-out (LODO) outer validation, in which each test fold is one complete measurement date and the training folds comprise the remaining dates; hyperparameters are tuned by an inner GroupKFold grid search grouped by date within the training folds (Supplementary Methods S2). The same seven algorithms and four feature

sets were then used for the leave-one-vessel-identifier-out (LOVIO) and joint leave-out sensitivity analyses of Section 2.10.

The primary endpoint is within-date ranking discrimination between assigned adjacent formulations, not absolute nutrient-status diagnosis or the accuracy of classifying an individual plant with a transferable threshold. For each task the higher nominal supply level is the positive class, and ROC-AUC is computed directly from test-fold prediction scores without flipping scores or AUCs according to test labels. The date-averaged AUC answers "within a held-out date, can the model rank the vessels of two supply levels correctly"; a common shift of scores leaves that date's AUC unchanged but can markedly affect fixed-threshold classification, so the metric does not show that a single threshold classifies accurately across dates. $|\mathrm{AUC} - 0.5|$ is used only as a post hoc, direction-independent auxiliary descriptor of ranking strength and never to select, flip or re-report primary predictive performance. LODO training sets may include data after the test date, so LODO evaluates internal generalization to a held-out date, not future-time prediction (diagnostics in Supplementary Table S10; implementation limitations in Supplementary Methods S4(9)).

Statistical interpretation. For each held-out date, ROC-AUC was calculated from six vessel–date scores (three per formulation level). The primary date-averaged AUC is the arithmetic mean of the per-date AUCs, giving each date equal weight rather than pooling predictions across potentially shifted dates. 95% date-cluster bootstrap intervals were obtained by resampling dates from fixed out-of-fold predictions; models were not refitted. Each date contributes nine positive–negative score pairs, so its AUC changes by 1/9 without ties or by half-steps of 1/18 when ties occur. Date averaging permits smaller increments; there is no universal 0.1 resolution threshold for the mean. An AUC below 0.5 indicates that the fitted model ranks the higher-supply class in the opposite direction more often than expected by chance. It does not show that the underlying sensor contains no information, and such AUCs were not reversed in the primary analysis.

2.8. Paired Uncertainty and Sensitivity Analysis

Logistic regression was the common reference algorithm for the paired sensor comparison, with the other six assessing model dependence; the logistic reference was chosen during analysis development rather than pre-registered, so the corresponding inference is exploratory. For the out-of-fold predictions, 1000 paired date-cluster bootstrap resamples were used to compute date-averaged AUCs and 95% percentile intervals of between-modality differences (all 168 "model × task" combinations in Supplementary Table S14). These are date-reweighting intervals conditional on fixed out-of-fold predictions: resampling reweights the observed dates and refits nothing, so the intervals exclude uncertainty from retraining, independent solution preparation and independent batches, and—because dates share vessel trajectories and outer training sets overlap heavily—do not remove those dependence structures. The date-elimination analysis carries the same caveat: it removes one date's score contribution rather than rerunning training and tuning, so it answers whether conclusions are driven by one date's scores, not whether retraining without that date would give the same conclusions. For each pre-specified modality pairing, the six "stage × adjacent interval" tasks form one exploratory testing family with Holm-adjusted sign-test p-values (Supplementary Table S11). We therefore mainly report effect sizes, conditional intervals and seven-algorithm direction counts: algorithms are not independent biological replicates, and an interval not crossing zero is not confirmatory evidence at the independent-preparation level; at 6 date clusters the interval is better read as empirical dispersion across the observed dates than as nominal 95% confidence (Supplementary Methods S4; per-fold distributions in Supplementary Table S7).

2.9. Weather-Related Temporal Predictability

Recorded air temperature, relative humidity, wind speed, and precipitation were used to predict date-mean electrical responses. Relative to a leave-one-date-out training-set-mean baseline, predictive skill is defined as $1 - \frac{MSE_{\text{model}}}{MSE_{\text{baseline}}}$, with positive values indicating improvement over that baseline. This analysis characterizes the predictability of date-level variation; its results do not enter the modality comparison.

2.10. Vessel-Identifier Leave-Out and Joint Date–Vessel-Identifier Leave-Out

To examine sensitivity to the internal validation target, a leave-one-vessel-identifier-out (LOVIO) scheme was applied to the seven algorithms and four feature sets. For each task, all observations of one fixed vessel identifier (1, 2 or 3) in both formulations form the test set, giving three outer folds; identifiers were assigned randomly within each formulation and are not biological pairings, but remained fixed throughout tracking so that longitudinal trajectories stay consistently grouped. All preprocessing and hyperparameter selection used training records only, and the inner GroupKFold grouped records by the two remaining vessel identifiers (two folds) rather than by date as in LODO, which limited tuning stability. LOVIO answers the internal generalization question "a new, unseen vessel within the same batch," complementary to LODO's "unseen date." As in the joint leave-out, out-of-fold predictions are pooled across the three outer folds, so LOVIO AUCs may likewise be affected by cross-model score-scale differences; both schemes are exploratory internal sensitivity analyses (Supplementary Table S13).

Because identifiers were randomly assigned within treatments, their cross-formulation combination was examined by a bottle-number remapping audit—that is, a random reassignment of vessel identifiers within each treatment, carried out to test whether the results depend on which vessel identifier was paired with which, rather than to generate new data: holding each vessel's longitudinal observations fixed, all six one-to-one mappings of the three bottle numbers of the higher level relative to the lower level were refitted for three algorithms (logistic regression, LinearSVM, RBFSVM), four feature sets and six tasks, giving 432 evaluations. Score types and aggregation are identical to the original LOVIO, but after remapping the inner GroupKFold groups by the two remaining bottle numbers rather than by training dates. Scores from different outer fits are still pooled across folds, so this is a remapping sensitivity analysis under identical definitions, not a replication free of cross-model score-scale differences (0 failures; Supplementary Data S1 and Data S2).

A joint date–vessel-identifier leave-out was further conducted for logistic regression: training excluded the observations of the test date and all observations of the test identifier, giving 30 "date × identifier" outer test combinations per vegetative task and 18 per reproductive task. Each fold has only two test observations, so single-fold AUC can only be 0, 0.5 or 1; the scheme therefore pools the three held-out identifiers of each date, computes a per-date AUC and averages. The three identifiers correspond to three different outer fitted models, so pooling may affect ranking through cross-model score-scale differences, and the joint leave-out is used only as an exploratory internal sensitivity analysis.

2.11. Computing Environment

All analytical workflows were implemented in Python 3.10.20. Data processing and record aggregation used pandas and NumPy; all classification models (logistic regression, linear and RBF-kernel support vector machines, random forest, extra trees, k-nearest neighbors, and histogram-based gradient boosting), the nested leave-one-date-out validation, and the inner GroupKFold hyperparameter grid searches were implemented with scikit-learn; correlation and distribution-based statistics used SciPy; figures were prepared with matplotlib.

3. Results

3.1. Between-Vessel Variation Under the Two Sampling Schemes

Under the two joint sampling schemes—third leaf in the vegetative stage and flag leaf in the reproductive stage—the empirical between-vessel dispersion of the five electrical descriptors differed, being consistently higher in the former, with ratios ranging from 1.37-fold for ICP (3.36 vs. 2.45) to 2.25-fold for IR (5.20 vs. 2.31), and 1.87-, 1.80-, and 1.42-fold for IZ, IXl, and IXc, respectively (Table 3, Figure 3). The within-stage ranking of the five descriptors was not consistent between stages: IR and IXl were the two largest in the vegetative stage (5.20 and 5.11), whereas IXl was largest (2.84) and IZ smallest (2.19) in the reproductive stage, with IXc and ICP tied next (both 2.45). The reproductive-stage estimates of IXc and ICP coincide to three decimals, and the two are linked analytically at 3 kHz (Supplementary Methods S4), so they are not two independent information sources here; we retain both only because they enter Electrical5 as separate channels. Because R is expressed against the pooled within-cell reference, these ratios mean that vessel-to-vessel scatter within a date and supply level was roughly 1.4–5.2 times the within-cell reference dispersion in the vegetative stage and 1.0–2.3 times it in the reproductive stage, indicating substantial vessel-level dispersion relative to the pooled within-cell reference; the separate contributions of biological and measurement-related variation cannot be determined from these ratios.

Table 3. Between-vessel dispersion ratios of the five zero-force electrical descriptors by sampling stage: within-group dispersion on the log scale over three vessels on the same date and supply level, relative to the pooled within-cell reference; parentheses give 95% date-cluster bootstrap intervals. Vegetative stage: 40 contributing dates of 42 recorded; reproductive stage: 29 dates, all retained though two have incomplete level coverage (22 January 2026 with 2 of 4 levels, 24 June 2026 with 3 of 4). Dates with partial coverage contribute only the computable cells. The stages differ in leaf position and their dates are unpaired, so stage and leaf-position effects cannot be separated.

Electrical Descriptor	Vegetative Dispersion Ratio (95% CI)	Reproductive Dispersion Ratio (95% CI)
IR	5.20 (4.03–6.54)	2.31 (2.01–2.71)
IZ	4.09 (3.33–5.06)	2.19 (1.97–2.46)
IXc	3.49 (3.09–3.94)	2.45 (2.13–2.75)
IXl	5.11 (4.15–6.40)	2.84 (2.43–3.33)
ICP	3.36 (2.97–3.77)	2.45 (2.18–2.74)

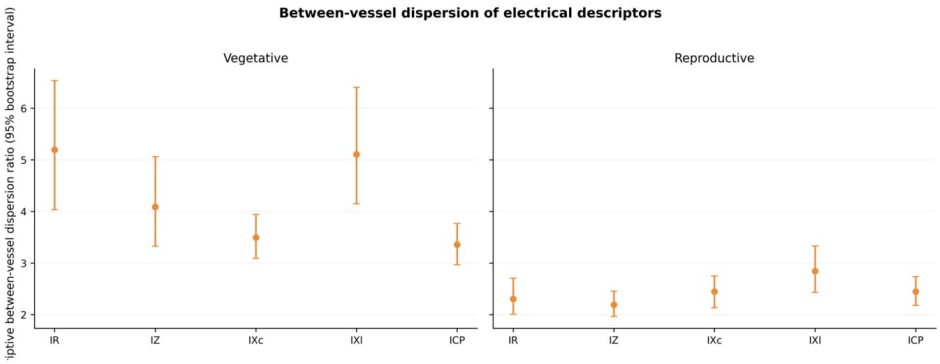


Figure 3. Between-vessel dispersion ratios of the five zero-force electrical descriptors in the vegetative (third leaf, 40 contributing dates of 42) and reproductive (flag leaf, 29 dates, two with incomplete level coverage) stages; partial dates contribute only the computable dispersion cells. Points are stage summary estimates; error bars are 95% date-cluster bootstrap intervals of the fixed aggregates. The stages differ in leaf position and date composition and are not a paired comparison. Take-home: within-group dispersion among vessels differed between developmental stages, but the contributions of biological variation, electrode contact, and instrument-related factors could not be independently separated.

Lower between-vessel dispersion was observed under the reproductive-stage flag-leaf scheme (44–73% of that under the vegetative-stage third-leaf scheme), but this cannot be attributed independently to leaf position or growth stage, which were confounded with measurement date and environmental conditions, and lower dispersion does not by itself establish superior discrimination or greater threshold stability. Any future threshold based on electrical measurements should therefore specify its applicable growth stage, leaf position and measurement conditions.

3.2. The Discriminative Advantage of the Two Modalities Reverses Across Supply Intervals

Under nested leave-one-date-out (LODO) validation, the paired modality differences of the logistic reference model showed a clear interval reversal in the reproductive stage (Figure 4a): in the 25–50% interval IR showed higher internal discrimination, with a date-averaged AUC difference (IR − SPAD) of +0.296 (95% date-cluster bootstrap interval +0.092 to +0.491), corresponding to an IR AUC of 0.870 against 0.574 for SPAD; in the 75–100% interval SPAD showed higher internal discrimination, with a difference of −0.630 (interval −0.871 to −0.352), corresponding to a SPAD AUC of 0.981 against 0.352 for IR (original direction; Section 2.7); in the 50–75% interval the two were essentially tied (+0.009; −0.194 to +0.259). Neither endpoint contrast has a bootstrap interval that includes zero. This reversal is the central empirical observation of this study: on the same leaves in the reproductive stage, each modality achieved a relatively high internal AUC in one endpoint interval (0.870 for IR, 0.981 for SPAD) while the other ranked substantially weaker under the same reference model.

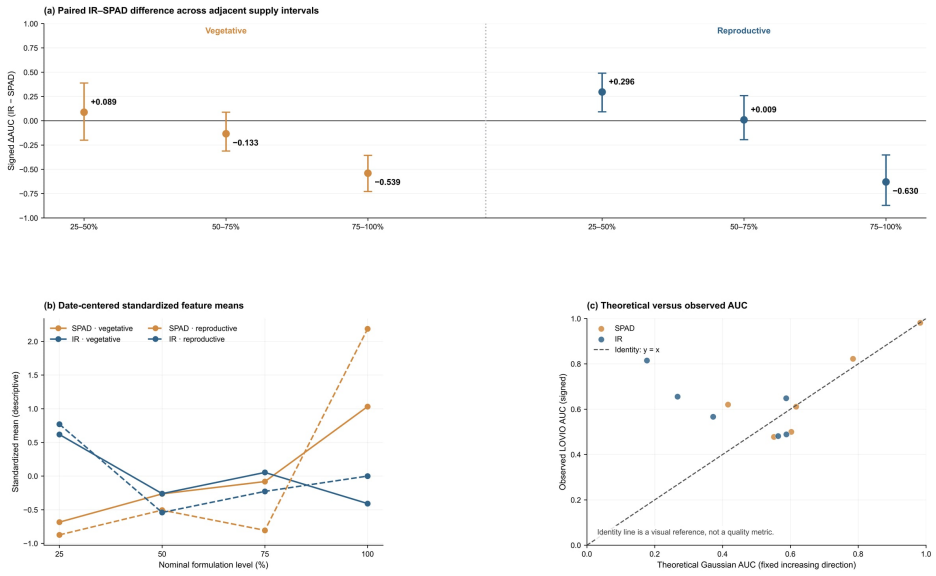


Figure 4. Interval-dependent IR–SPAD discrimination and descriptive response patterns. (**a**) Paired differences in date-averaged ROC-AUC (IR − SPAD) for the logistic reference model under nested leave-one-date-out (LODO) validation; whiskers show 95% date-cluster bootstrap intervals obtained by reweighting fixed out-of-fold predictions. Positive values favor IR and negative values favor SPAD. (**b**) Date-centered standardized mean responses at each nominal supply level (IR analyzed on the log scale). Adjacent differences in these descriptive curves define marginal separation, d; they are not cross-validated classifier predictions. (**c**) Theoretical AUC under an equal-variance normal approximation and a fixed increasing-score direction (horizontal axis) versus observed date-averaged leave-one-vessel-identifier-out (LOVIO) AUC under the predefined higher-supply positive label (vertical axis; 12 stage–interval–feature cells). The dotted diagonal is the identity line (y = x), indicating exact numerical agreement rather than a model-performance threshold. The theoretical AUC does not use the post hoc direction that maximizes separation. Take-home: the paired ranking reverses between the reproductive endpoint intervals (**a**), the marginal response patterns differ across formulations (**b**), and marginal separation alone does not determine cross-validated AUC (**c**).

The primary analysis retains the prespecified higher-supply positive-label direction. Supplementary Table S3 also reports the descriptive, direction-independent transformation $|AUC - 0.5| + 0.5$, applied after date averaging without refitting. For the vegetative 50–75% contrast, this transformation changes the apparent ordering (original AUC: IR 0.333, SPAD 0.467; transformed values: IR 0.667, SPAD 0.533). Because the direction is selected after observing the result, the transformed values are not estimates of deployable predictive performance. Primary conclusions therefore use the original-direction AUC.

The corresponding original and transformed values are provided in Supplementary Table S3.

3.3. Seven-Model Comparison: Directional Agreement Varies by Interval

The seven classifiers did not agree uniformly, and the pattern of disagreement varied by interval (Table 4, Figure 5). Two of the six tasks were unanimous: the vegetative 25–50% interval favored IR (7/0/0) and the reproductive 75–100% interval favored SPAD (0/7/0). The reproductive 25–50% interval was least stable, with IR − SPAD ranging from +0.296 (logistic regression and linear SVM: 0.870 against 0.574) to −0.065 (random forest: 0.694 against 0.759), giving four positive, two negative and one tie. Feature representation mattered independently of modality: in the vegetative 50–75% interval the date-averaged AUCs were 0.467 for SPAD, 0.333 for IR, 0.689 for Electrical5 and 0.644 for Fusion, so all seven classifiers favored Electrical5 over SPAD while only five favored IR—a single reference algorithm cannot summarize this interval. All classifiers were fitted to the same matched records, so the counts characterize sensitivity to modeling choices, not seven independent replications; direction conventions follow Section 2.7.

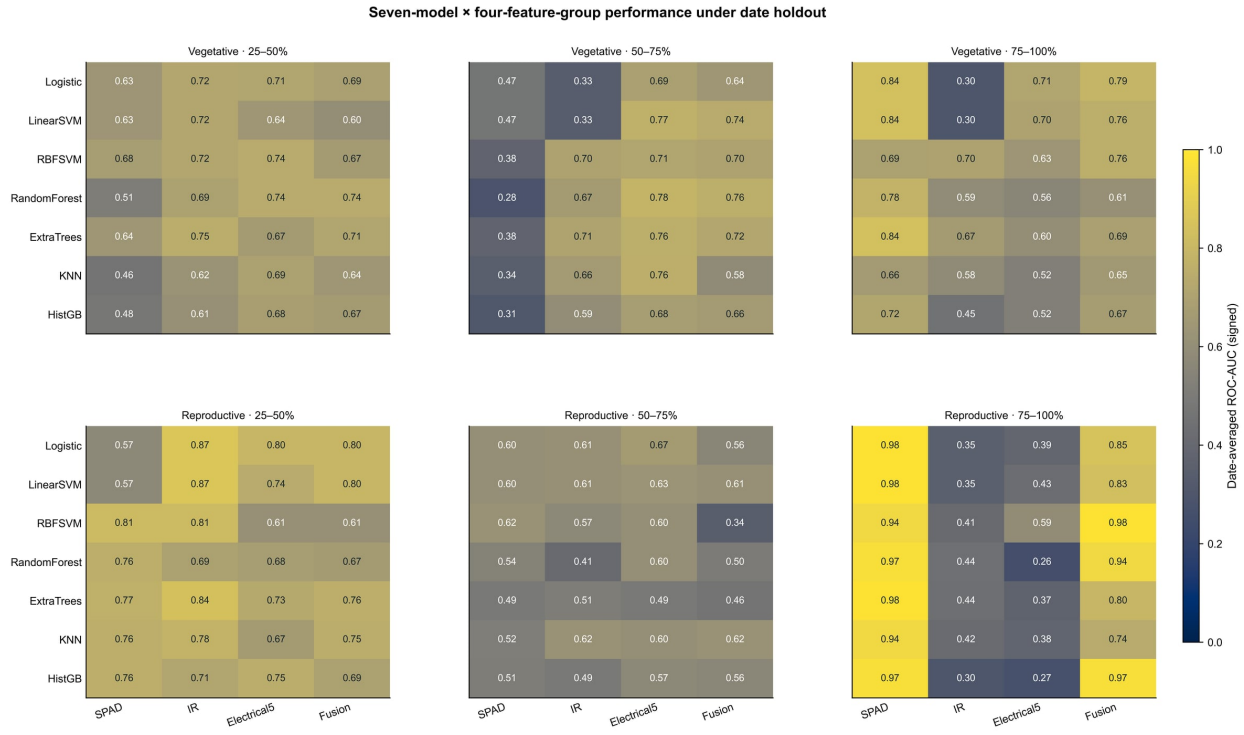


Figure 5. Nested-LODO date-averaged ROC-AUC of seven classifiers and four feature sets across three adjacent supply intervals in two stages (168 combinations). Color scale 0–1; AUCs are not flipped according to test labels; SPAD, IR, Electrical5 and Fusion are feature sets, not four independent modalities. Two decimals are for display only; Table 4 uses unrounded AUCs. Take-home: where algorithms disagree across adjacent intervals, the ranking depends on the classifier as much as on the modality.

Table 4. Direction counts of modality pairings for seven classifiers under nested leave-one-date-out validation. "Positive/negative/tie" count the classifiers whose date-averaged ROC-AUC for IR (or Electrical5) is higher or lower than that of SPAD; the three sum to 7. Counts use unrounded differences, with $|\Delta AUC| \leq 1 \times 10^{-10}$ counted as a tie. They characterize sensitivity to modeling choices, not seven independent replicates; AUCs below 0.5 retain the original direction relative to the higher-supply label and are not flipped.

Growth Stage	Supply Interval	IR − SPAD: Positive/Negative/Tie	Electrical5 − SPAD: Positive/Negative/Tie
Vegetative	25–50%	7/0/0	7/0/0
	50–75%	5/2/0	7/0/0
	75–100%	1/6/0	0/7/0
Reproductive	25–50%	4/2/1	2/5/0
	50–75%	4/3/0	5/1/1
	75–100%	0/7/0	0/7/0

3.4. Analytical Mapping Between Standardized Marginal Separation and Internal Discrimination

To describe the marginal separation of the two single-variable measurements between adjacent supply levels, date-centered standardized means were computed from the B2 matched records. Within each date, the same-day mean of the modality's four supply levels was subtracted, and the difference between the centered residual means of adjacent levels was divided by the pooled within-group standard deviation of the four levels, giving the signed separation d; IR uses the log scale. If the single-variable distributions of two adjacent levels are approximately normal with equal variance, the theoretical AUC with the pre-fixed direction "larger feature values indicate higher supply" is $AUC = \Phi\frac{d}{\sqrt{2}}$, and the direction-independent theoretical separation is $AUC = \Phi\frac{|d|}{\sqrt{2}}$, where $d = \frac{\mu_{high}-\mu_{low}}{\sigma}$. Both quantities are marginal-distribution approximations and cannot be equated with the out-of-fold AUC of a trained classifier.

Figure 4c plots the theoretical AUC under the pre-fixed direction "higher feature values indicate higher supply" against the observed date-averaged LOVIO AUC; across the 12 "stage × interval × modality" cells, the same-batch association is weak (Pearson r = 0.312, Spearman ρ = 0.154, mean absolute difference 0.157). Choosing the better direction post hoc per cell raises it to r = 0.938 and ρ = 0.818 (mean absolute difference 0.054), but that is not the definition plotted and cannot be read as predictive ability under a pre-fixed direction or as a prospective rule for modality selection (per-cell σ, d and both conventions in Supplementary Table S2).

The standardized marginal separation of IR and SPAD crosses between adjacent supply intervals is consistent with the modality-ranking changes observed in internal validation. This is a distributional explanation, not a causal mechanism or an externally validated rule; marginal separation cannot summarize multivariate joint distributions, tuning fluctuation or cross-date transfer, and the analysis uses only B2 matched records.

3.5. Interval-Dependent Modality Rankings and the Limited Benefit of Feature Fusion

Under nested LODO with the logistic reference algorithm, Fusion did not exceed the best non-fused feature set in any of the six "stage × interval" tasks (Table 5, Figure 6); the AUC differences are −0.033, −0.044 and −0.050 in the vegetative stage and −0.074, −0.111 and −0.130 in the reproductive stage. The relative advantage of the two modalities therefore changes with the target supply interval, but at the current sample size, feature definitions and reference algorithm, simple concatenation produced no stable within-interval gain. Electrical5 and IR each lead in some tasks, and the electrically derived features are highly correlated, which indicates that IR is a competitive parsimonious benchmark rather than

proving that the remaining electrical features carry no independent information. The best non-fused set is chosen post hoc from the same data, so this does not validate a deployment strategy or exclude gains under other algorithms, fusion methods or independent batches.

Table 5. Date-averaged ROC-AUC of the logistic reference model under nested leave-one-date-out validation (6 "stage × interval" tasks; the four feature sets and the IR − SPAD difference). Δ(IR − SPAD) is IR minus SPAD; positive values favor IR. All values are given to three decimals; Δ is computed from unrounded values, so subtracting the listed values may differ by ±0.001.

Growth Stage	Supply Interval	SPAD	IR	Electrical5	Fusion	Δ (IR − SPAD)
Vegetative	25–50%	0.633	0.722	0.711	0.689	+0.089
	50–75%	0.467	0.333	0.689	0.644	−0.133
	75–100%	0.839	0.300	0.711	0.789	−0.539
Reproductive	25–50%	0.574	0.870	0.796	0.796	+0.296
	50–75%	0.602	0.611	0.667	0.556	+0.009
	75–100%	0.981	0.352	0.389	0.852	−0.630

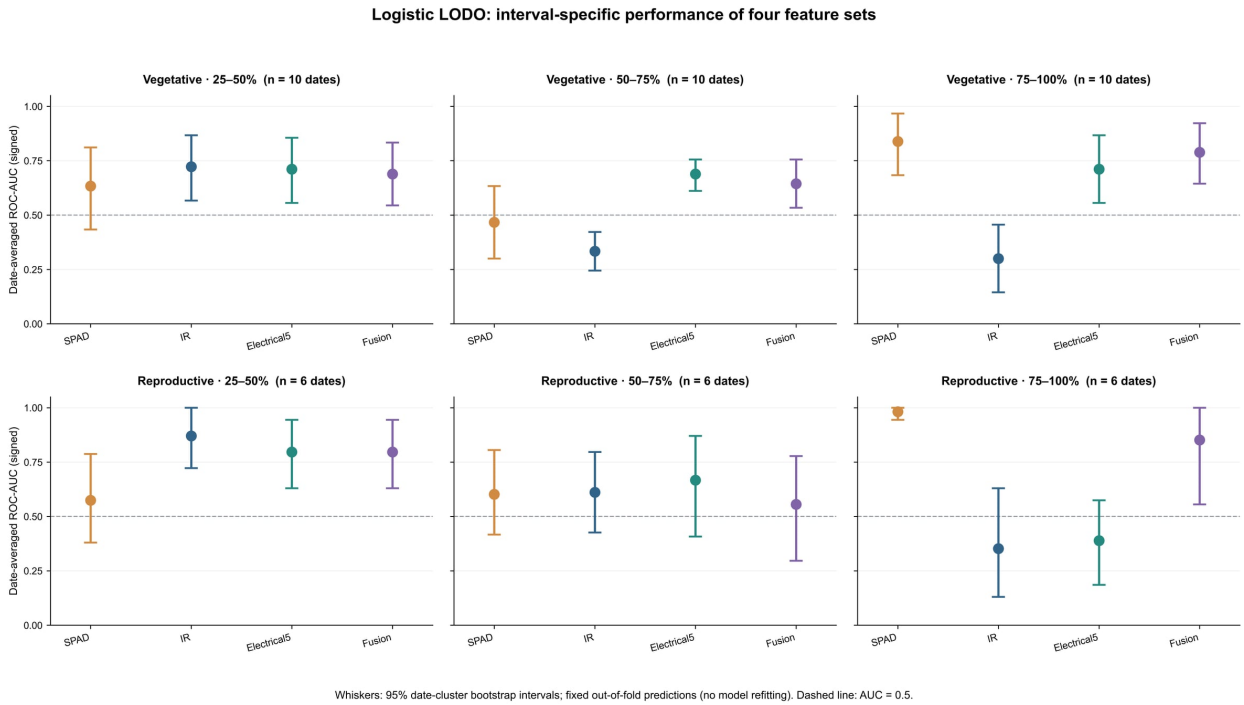


Figure 6. Logistic-regression discrimination across six growth-stage × supply-interval tasks under nested leave-one-date-out validation. Points show date-averaged ROC-AUC for SPAD, IR, Electrical5, and Fusion; whiskers show 95% date-cluster bootstrap intervals obtained by reweighting fixed out-of-fold predictions without model refitting. Intervals may be wider in the reproductive stage because only six dates contribute, compared with ten vegetative-stage dates; width also depends on between-date variability. Fusion did not exceed the strongest non-fused feature set in any of these six tasks, and no feature set led across all tasks. Take-home: in these six tasks simple concatenation gave no consistent gain over the best non-fused feature set, and no feature set led throughout, so the advantage is task-specific rather than a property of the feature set. These comparisons do not establish the same ordering under other validation schemes.

3.6. The Predictive Value of Recorded Weather Conditions Varies by Stage and Descriptor

Relative to a leave-one-date training-set-mean baseline, the predictive skill of air temperature, relative humidity, wind speed, and precipitation state for date-mean electrical

descriptors differs by stage (Supplementary Figure S1; 42 vegetative and 29 reproductive dates, i.e., all recorded dates, including those with incomplete level coverage specified in the figure caption). Four descriptors are positive in the reproductive stage (IXc +0.385, IZ +0.363, IXl +0.190, IR +0.155), with ICP at −0.027; in the vegetative stage, only ICP is slightly positive (+0.063). This analysis describes only the predictable component of date-level variation and provides no evidence of meteorological causation or of classification gains from environmental correction.

3.7. Key Differences, Validation Sensitivity, and Algorithm Dependence Under Three Internal Leave-Out Schemes

Three internal leave-out schemes were compared: LODO excludes dates, LOVIO excludes vessel identifiers, and joint leave-out excludes both (Tables 6 and 7, Figure 7). All reuse the B2 records and are internal sensitivity checks rather than independent validation; because they differ in test targets and in cross-fold score aggregation, their magnitudes should not be compared as better or worse. The key logistic contrasts keep their direction throughout—reproductive IR − SPAD is +0.296, +0.315 and +0.352 for 25–50% and −0.630, −0.500 and −0.685 for 75–100% under LODO, LOVIO and joint leave-out, and vegetative Electrical5 − SPAD is +0.222, +0.111 and +0.244 for 50–75%—with 95% date-cluster bootstrap intervals (1000 resamples, same conventions as Table 5 and Section 3.2) of, in order, reproductive 25–50% +0.092 to +0.491, +0.185 to +0.463 and +0.185 to +0.519 and reproductive 75–100% −0.871 to −0.352, −0.778 to −0.222 and −0.889 to −0.463; all 12 rows are listed in Table 6. Bottle-number remapping produced no failures across 432 refits, and the sign of the IR − SPAD contrast in the two reproductive endpoint intervals never changed across the six identifier mappings (Supplementary Methods S4); the mappings are not independent replicates. LOVIO direction counts diverge from LODO in detail (Table 7, Supplementary Figure S2): all seven classifiers favor IR over SPAD in the reproductive 25–50% interval under LOVIO against four of seven under LODO, whereas all seven favor SPAD in the reproductive 75–100% interval under both. This discrepancy reflects leave-out granularity—LOVIO admits other vessels of the test date into training—rather than instability of the endpoint conclusion.

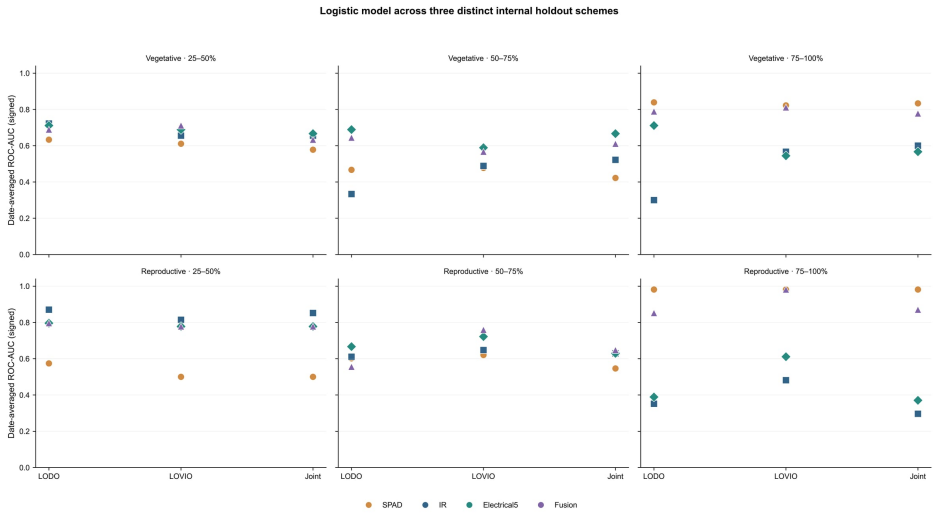


Figure 7. Date-averaged ROC-AUC of the logistic reference model under three internal validation schemes—LODO, LOVIO and joint date–vessel leave-out—grouped by "stage × interval × feature set." The horizontal categories are different leave-out targets, not ordered exposures, and their spacing carries no metric meaning; all schemes reuse the same B2 matched records and are not external validation. Take-home: the direction and rough size of the endpoint contrasts survive all three leave-out targets.

Table 6. Date-averaged ROC-AUC of logistic regression under three internal leave-out schemes: LODO (leave-one-measurement-date-out, Table 5), LOVIO (leave-one-vessel-identifier-out), and joint leave-out (excludes the test date and all records of the test identifier). Δ is IR minus SPAD; positive values favor IR. All tasks use the same B2 matched records from 10 vegetative and 6 reproductive dates, so the schemes cannot serve as independent validation. Conventions and rounding are as in Table 5; the 95% date-cluster bootstrap intervals of Δ (1000 resamples, seed 20261010) follow Section 3.2, and with very few test observations per fold under LOVIO and joint leave-out, their widths should not be compared directly with LODO.

Growth Stage	Supply Interval	Validation	SPAD	IR	Electrical5	Fusion	IR − SPAD	95% Interval for Δ
Vegetative	25–50%	LOVIO	0.611	0.656	0.689	0.711	+0.044	−0.200 to +0.278
		Joint leave-out	0.578	0.656	0.667	0.633	+0.078	−0.167 to +0.322
	50–75%	LOVIO	0.478	0.489	0.589	0.567	+0.011	−0.178 to +0.222
		Joint leave-out	0.422	0.522	0.667	0.611	+0.100	−0.056 to +0.311
	75–100%	LOVIO	0.822	0.567	0.544	0.811	−0.256	−0.444 to −0.078
		Joint leave-out	0.833	0.600	0.567	0.778	−0.233	−0.433 to −0.044
Reproductive	25–50%	LOVIO	0.500	0.815	0.778	0.778	+0.315	+0.185 to +0.463
		Joint leave-out	0.500	0.852	0.778	0.778	+0.352	+0.185 to +0.519
	50–75%	LOVIO	0.620	0.648	0.722	0.759	+0.028	−0.120 to +0.204
		Joint leave-out	0.546	0.630	0.630	0.648	+0.083	−0.056 to +0.241
	75–100%	LOVIO	0.981	0.481	0.611	0.981	−0.500	−0.778 to −0.222
		Joint leave-out	0.981	0.296	0.370	0.870	−0.685	−0.889 to −0.463

Table 7. Number of classifiers whose date-averaged ROC-AUC supports each modality direction under leave-one-vessel-identifier-out (LOVIO) validation, out of 7 per cell. Counts indicate algorithm directions, not independent statistical replicates, and do not justify selecting the best-performing algorithm for deployment. They are computed from unrounded AUC differences (positive threshold $> 1 \times 10^{-10}$), not from the two-decimal values in Supplementary Figure S2.

Growth Stage	Supply Interval	LOVIO IR > SPAD	LOVIO Electrical5 > SPAD
Vegetative	25–50%	7/7	7/7
	50–75%	6/7	7/7
	75–100%	0/7	0/7
Reproductive	25–50%	7/7	7/7
	50–75%	5/7	7/7
	75–100%	0/7	0/7

3.8. Additional Date Sensitivity and Electrical-Feature Redundancy

Removing one date at a time preserved the sign of the reproductive-stage IR–SPAD difference in the two endpoint intervals (25–50%: +0.233 to +0.367; 75–100%: −0.733 to −0.556). These are within-B2 sensitivity checks, not independent replications; detailed results are provided in the Supplementary Results S17.

3.9. Growth (Plant-Height) Control Analysis

Plant-height analyses were exploratory sensitivity checks using the 192 paired B2 observations, not independent tests of nutrient-status information. The unadjusted interval-dependent reversal is the primary finding under the original measurement and validation conditions. Plant height is a growth-vigor trait associated with assigned supply treatments; adjustment therefore changes the estimand and cannot be interpreted as isolating a causal nutrient-specific sensor signal. Detailed comparisons are provided in Supplementary Results S17.

The two reproductive endpoint contrasts were +0.296 and −0.630 before adjustment. After within-training-fold height residualization, they attenuated to +0.204 (95% bootstrap interval −0.074 to +0.444) and −0.204 (95% bootstrap interval −0.630 to +0.241). Thus, the opposite directions remained descriptive, but both bootstrap intervals included zero; the observed reversal cannot be claimed to survive adjustment for vigor. Plant height alone achieved a date-averaged AUC of 1.000 in two of six tasks, and adding height to the reproductive 75–100% models produced AUC 1.000 across feature sets, eliminating the modality contrast. These checks indicate that growth-vigor-associated information may contribute materially to the original sensor ranking; they do not invalidate discrimination between assigned formulations, which is the stated primary endpoint.

3.10. Cross-Batch Stability of the Electrical Modality Itself in an Independent Batch (B1)

B1 provides an independent electrical-only comparison, whereas the paired optical–electrical ranking was evaluated only in B2. The batches differed in season, measurement timing, and environmental conditions, while sharing the same outdoor-greenhouse hydroponic cultivation system; B1 has no SPAD records. Consequently, B1 can test the repeatability of electrical interval patterns across contexts but cannot independently validate or invalidate the B2 dual-modality reversal.

Under the same aggregation convention, B1 electrical-only discrimination showed a different interval-dependent pattern from B2 (Supplementary Table S6 continued). Of twelve stage × interval × electrical-feature-set comparisons, six were directionally concordant, five discordant, and one at chance. In B1, reproductive IR discrimination reached a date-averaged AUC of 0.693 (95% interval 0.534–0.831; $p = 0.022$) for 25–50% and 0.714 (0.582–0.841; $p = 0.004$) for 75–100%, whereas the latter B2 IR result was 0.352. These findings show heterogeneous electrical-only discrimination across the observed batches, not absence of useful electrical information in B1. Because B1 has no SPAD measurements, they cannot establish whether the relative optical–electrical modality ranking, or its reversal, transfers across batches. Both batches used outdoor-greenhouse hydroponics but differed in season, measurement timing, and environmental conditions.

3.11. Destructive Tissue Audit (Supplementary Results S17)

The 36 destructive tissue samples were not used for classification. Tissue-nitrogen variance was dominated by measurement date ($\eta^2 = 0.889$) rather than treatment ($\eta^2 = 0.016$); these data do not independently validate sensor rankings (Supplementary Table S5 and Results S17).

4. Discussion

4.1. Interval-Dependent Discrimination and Its Implications for Sensor Evaluation

In the B2 paired data, the two reproductive endpoint intervals show opposite modality rankings: IR ranked above SPAD in the 25–50% interval and below it in the 75–100% interval. The practical consequence is that a pooled, whole-gradient summary can conceal a difference between adjacent contrasts, so any stated advantage is conditional on the interval examined. An AUC below 0.5 means the fitted scores ranked the higher-supply class below chance; it is a property of the fitted model under the pre-set direction and does not establish that the raw feature lacks information (Section 2.7). The weight the reversal can carry is set by the bounds listed in Section 4.5.

4.2. Three Candidate Sources of the Ranking Reversal

Several non-exclusive explanations remain possible. The nominal formulations changed N, K, and Ca jointly, and date-centered SPAD and log-IR profiles differed across

supply intervals (Figure 4b). The nominal K:N ratio also changed unevenly between adjacent formulations (approximately 0.600 at 25% and 0.400 at 100%, with Ca:N approximately 0.267). These compositional differences provide a possible context for the observed sensor ranking reversal. Because the three elements were varied jointly, the resulting compositional shift may have directly influenced membrane-related electrical properties, ionic conductivity, and tissue polarization independently of any nitrogen-specific physiological response, so that part of the electrical signal could reflect generic ionic and membrane-level effects rather than nitrogen status. On the optical side, light-dependent chloroplast movement has been reported to shift SPAD readings at low nitrogen supply [33]; we did not measure chloroplast movement or leaf optical properties and cannot attribute that mechanism to the present results. Elemental supplies were not independently manipulated, however, and tissue K concentrations and membrane-related electrical mechanisms were not measured; the K:N interpretation therefore remains a hypothesis, not an identified mechanism, and the data cannot attribute the reversal to a single element or physiological process.

4.3. Implications for Sensor Benchmarking in Controlled Nutrient-Supply Systems

These results inform early-stage selection of sensor representations for controlled formulation-contrast experiments. Electrical acquisition used a dedicated LCR meter, electrodes, and force-dependent measurements followed by extrapolation, whereas SPAD required a handheld optical reading; this difference implies different demands on operator time, calibration, hardware, and data processing. Technological innovation should be judged not only on technical performance but also on its agronomic and economic return [34]; we did not quantify throughput, equipment costs, labor, power demand, or agronomic benefit, so no economic superiority or commercial feasibility can be claimed.

For practical sensor benchmarking, ROC-AUC rankings should be distinguished from calibrated decision thresholds. An operational threshold would need prospective calibration and validation for a specified agronomic decision, rather than selection from the observed formulation contrasts. These requirements help define the next steps for translating interval-dependent discrimination into a usable monitoring procedure.

4.4. An Evidence-Informed Four-Dimension Reporting Framework

The principal empirical contribution is the observation that relative sensor discrimination varied across predefined formulation contrasts: in the paired B2 data, the reproductive-stage IR–SPAD ranking reversed between the lower and higher adjacent supply intervals under the same reference classifier and validation scheme. A modality that performs favorably for one predefined treatment contrast may not retain that advantage for another, so a single overall performance estimate cannot summarize such comparisons.

We synthesize the observed dependencies into an evidence-informed reporting framework, not a validated sensor-selection algorithm. Comparisons should specify (1) the predefined target formulation interval and growth stage; (2) modality, feature representation, and classifier; (3) validation target and uncertainty procedure; and (4) evidence for independent cross-batch replication. The paired B2 data address the first three dimensions; B1 provides electrical-only batch context for the fourth and cannot test cross-batch transfer of the optical–electrical ranking. The framework is a transparent reporting recommendation rather than proof that using it improves deployment performance.

4.5. Limitations and Scope of Inference

The bounds below apply to every result in this paper; they are stated once here rather than repeated in each result. In brief, all internal checks reuse the B2 records, so none of the leave-out, remapping, or date-elimination analyses is external validation [29]; the models

were scored on different score conventions (the two SVMs by decision_function, logistic regression by positive-class probabilities, always in the pre-set positive direction), so cross-model AUC magnitudes are not directly comparable [27,35]; and algorithmic agreement reflects sensitivity to modeling choices, not independent replication.

Relatedly, within-group dispersion among vessels mixes plant differences, rhizosphere microenvironment, electrode contact and instrument factors, and this design lacks the independent repeated measurements needed to decompose those components. Meteorological predictability of some reproductive-stage date means indicates a predictable component in date drift but does not prove a causal role, and we did not test whether environmental correction improves classification [25,26,36].

Supplementary Analysis S18 characterizes the measured temperature support for the two outdoor-greenhouse hydroponic batches. The vegetative-stage temperature ranges overlapped only at 15–17 °C, while reproductive-stage ranges did not overlap. None of the 80 within-batch, stage- and formulation-stratified date-level Spearman tests reached nominal $p < 0.05$. These exploratory results do not establish temperature independence or identify the causes of batch differences, because the number of dates was limited and temperature covaried with season and measurement timing.

The specific limitations are as follows.

(1) Covarying elements. N, K and Ca were varied jointly, so a supply level denotes a formulation proportion rather than a single-element dose, and K:N stoichiometry changed together with the dose (Section 4.2). No element-specific mechanism can be isolated.

(2) Replication structure. The three vessels of a formulation shared one solution preparation at each renewal, and the two plants per vessel were not tracked independently; preparation-level effects therefore cannot be separated from treatment-associated discrimination.

(3) Single dual-modality batch. The paired comparison rests on B2 alone. B1 is electrical-only, so it tests the electrical modality across batches but not the relative ranking of the two modalities.

(4) Analysis-dependent choices. The logistic reference algorithm was selected during analysis development rather than pre-registered, so the associated *p*-values and intervals are exploratory; Holm adjustment covers only the six tasks within each pre-specified modality pairing and does not remove multiplicity across all exploratory comparisons [28,37].

(5) Conditional uncertainty. The date-cluster bootstrap resamples fixed out-of-fold predictions and therefore excludes uncertainty from model retraining, solution preparation and external batches.

(6) Resolution of the primary metric. Each held-out date provides six scores (three per class), giving nine positive–negative comparisons; the per-date AUC changes in steps of 1/9 without ties or 1/18 with half-credit for ties. Date averaging can yield smaller steps, and the limited date and vessel counts—not a universal 0.1 cutoff—constrain precision (Section 2.7).

(7) Vigor confounding. Plant height alone reached a date-averaged AUC of 1.000 in two of the six tasks; after within-training-fold height residualization the two reproductive endpoint contrasts attenuate to +0.204 (95% bootstrap interval −0.074 to +0.444) and −0.204 (95% bootstrap interval −0.630 to +0.241), both now including zero, so the reversal should be read as a directional pattern rather than as an effect that survives adjustment for vigor (Section 3.9).

(8) Destructive biochemistry. Tissue-nitrogen variance was dominated by sampling date ($\eta^2 = 0.889$) rather than treatment ($\eta^2 = 0.016$), so these 36 samples are retained only as a traceability audit archive and enter no discrimination model (Section 3.11, Supplementary Table S5).

(9) Season–batch confounding. B1 and B2 shared outdoor-greenhouse hydroponics but differed in season, measurement timing, and temperature support; the S18 exploratory associations cannot isolate temperature effects (Supplementary Analysis S18).

(10) Measurement provenance. Preparation-time pH/EC checks were not archived and the generally SPAD-first acquisition order was neither randomized nor verified for every observation, limiting inference about solution chemistry and possible contact or order effects; and because the original eight-level force–electrical readings are not in the public supplement, the zero-force descriptors cannot be recomputed record by record from the archive.

(11) Scope. The study provides no element-specific diagnosis, no field extrapolation, and no deployment thresholds.

5. Conclusions

In the paired B2 winter-wheat experiment, the relative discrimination of electrical resistance (IR) and optical SPAD differed across adjacent compound mineral supply intervals. Under reproductive-stage logistic regression with leave-one-date-out validation, the date-averaged IR − SPAD AUC difference was +0.296 for 25–50% but −0.630 for 75–100%. Other comparisons depended on classifier, feature representation, and validation scheme. Fusion did not exceed the strongest non-fused representation in the six logistic reference-model tasks. Electrical-only patterns differed between B1 and B2; an independent paired batch is still needed to assess whether the optical–electrical reversal replicates. We recommend reporting the target interval, feature–classifier specification, validation design, and cross-batch evidence in leaf-sensor benchmarks. These results are a preliminary, condition-dependent sensor comparison rather than a validated diagnostic tool; they describe discrimination among assigned compound formulations, not validated nutrient diagnosis or fertilizer-management thresholds.

Supplementary Materials: The following supporting information can be downloaded at https://www.mdpi.com/article/10.3390/agronomy16212231/s1, The complete list of captions is given below and is identical to the revised SM file. Figure S1. Weather-related predictive skill for date-mean electrical descriptors, relative to a leave-one-date-out training-set-mean baseline, in the vegetative (n = 42 dates) and reproductive (n = 29 dates) stages; positive values indicate improvement over the baseline, and no causal interpretation is implied. Figure S2. Leave-one-vessel-identifier-out paired feature-group contrasts (feature set minus SPAD) across seven classifiers, three adjacent supply intervals and two growth stages; colours show the signed date-averaged AUC difference, and the two methods are not independent validation schemes. Figure S18-1. Measured ambient temperature on each of the 71 stage–batch measurement dates, plotted by batch within the vegetative and reproductive stages; each symbol is one measurement date. Table S1. Fixed estimator settings and the hyperparameter grids searched for the seven classifiers. Table S2. Date-centred standardized marginal separation d of SPAD and IR between adjacent nominal supply levels, with the theoretical AUC under a fixed increasing direction and under the post hoc direction. Table S3. Signed date-averaged AUC and the direction-free transformation |AUC − 0.5| + 0.5 for all hold-out schemes, stages, intervals and feature sets. Table S4. Plant-height sensitivity: unadjusted, height-as-covariate and within-training-fold height-residualized AUCs, including the univariate AUC of height alone. Table S5. Individual biochemical observations for the 36 destructive samples, with the cultivation batch annotated row by row. Table S6. B1 electrical-only cross-batch comparisons with date-averaged AUC, 95% intervals and p values against random ranking. Table S7. Date-level leave-one-date-out AUC for SPAD, IR and Electrical5, with the IR − SPAD difference, for every held-out date. Table S8. Sample flow for the full electrical set and the matched optical–electrical set, by batch and growth stage. Table S9. Electrical parameter definitions: instrument channel, raw unit, fitted relation against clamping force, zero-force extrapolation expression, final unit and zero/outlier handling. Table S10. Out-of-fold score-output diagnostics for the seven classifiers (score type, number of combinations,

probability ranges and standard deviations). Table S11. Exploratory sign-test p values and Holm-adjusted p values for the six stage × interval tasks within each modality pairing. Table S12. Leave-one-date-out AUC after refitting the two support vector machines with probability = False. Table S13. Leave-one-vessel-identifier-out within-fit pairwise ranking sensitivity across the seven classifiers. Table S14. Sensitivity of the bootstrap intervals to the near-zero tolerance used when counting ties, across all 168 model × task combinations. Table S15. Reconciliation of the two sample-flow accounting conventions and the duplicate-key audit of the aggregated records. Table S16. Audit of the five derived electrical descriptors: record counts, missing values, zeros, negatives and observed ranges. Table S18-1. Measured temperature support of the two outdoor-greenhouse batches, by growth stage and batch. Table S18-2. Within-batch nominal Spearman correlations between the daily mean ambient temperature and the five electrical descriptors, for every batch, growth stage and nominal supply level (80 tests). Methods S1. Biochemical assays. Methods S2. Feature sets, algorithms and hyperparameter search. Methods S3. Clamping-force–electrical models and zero-force extrapolation. Methods S4. Implementation details, score outputs and reproducibility limitations. Results S17. Detailed counting, sensitivity and plant-height results. Analysis S18. Measured temperature support for the two outdoor-greenhouse batches.

Author Contributions: Conceptualization, S.Z.; methodology, S.Z. and B.Z.; software, S.Z. and X.D.; validation, S.Z. and B.Z.; formal analysis, S.Z., and X.H.; investigation, S.Z. and X.D.; resources, B.Z. and C.W.; data curation, S.Z.; writing—original draft preparation, S.Z. and B.Z.; writing—review and editing, B.Z. and C.W.; visualization, S.Z. and X.H.; supervision, C.W. and B.Z.; project administration, B.Z. and C.W.; funding acquisition, C.W. All authors have read and agreed to the published version of the manuscript.

Funding: This research was funded by: the Priority Academic Program Development of Jiangsu Higher Education Institutions (PAPD2023-87); Project of Faculty of Agricultural Equipment of Jiangsu University (NZXB20200102); Key and General Projects of Jiangsu Province (BE2022338); Jiangsu Province Modern Agricultural Machinery Equipment Technology Promotion Project (NJ2024-09).

Data Availability Statement: The original contributions presented in this study are included in the article/Supplementary Materials. Further inquiries can be directed to the corresponding authors.

Acknowledgments: During the preparation of this manuscript, the authors used ChatGPT(GPT-4o; OpenAI, San Francisco, CA, USA) for the purposes of language refinement. The authors have reviewed and edited the output and take full responsibility for the content of this publication.

Conflicts of Interest: The authors declare no conflicts of interest.

Abbreviations

The following abbreviations are used in this manuscript:

N	Nitrogen
R	Resistance
Z	Impedance
XC	Capacitive reactance
XL	Inductive reactance
CP	Physiological capacitance
IR	Intrinsic resistance
IZ	Intrinsic impedance
IXc	Intrinsic capacitive reactance
IXl	Intrinsic inductive reactance
ICP	Intrinsic physiological capacitance
RF	Random forest
CV	Cross-validation
SPAD	Soil-slant analysis development
KNN	K-nearest neighbors
SVM	Support vector machine
ROC-AUC	Receiver operating characteristic-area under the curve

LCR	Inductance-capacitance-resistance
EC	Electrical conductivity
LODO	leave-one-date-out
LOVIO	leave-one-vessel-identifier-out
MSE	Mean squared error
SD	Standard deviation
CI	Confidence interval
HistGB	Histogram-based gradient boosting
RBF	Radial basis function
K	Potassium
Ca	Calcium
NR	Nitrate reductase
NiR	Nitrite reductase
Fd-GOGAT	Ferredoxin-dependent glutamate synthetase
GS	Glutamine synthetase
DW	Dry weight
FW	Fresh weight
PO	Polyolefin
PET	Polyethylene terephthalate
RMS	Root mean square

References

1. Savary, S.; Willocquet, L.; Pethybridge, S.J.; Esker, P.; McRoberts, N.; Nelson, A. The global burden of pathogens and pests on major food crops. *Nat. Ecol. Evol.* **2019**, *3*, 430–439. [CrossRef]
2. Shiferaw, B.; Smale, M.; Braun, H.-J.; Duveiller, E.; Reynolds, M.; Muricho, G. Crops that feed the world 10. Past successes and future challenges to the role played by wheat in global food security. *Food Secur.* **2013**, *5*, 291–317. [CrossRef]
3. Singh, B.K.; Delgado-Baquerizo, M.; Egidi, E.; Guirado, E.; Leach, J.E.; Liu, H.; Trivedi, P. Climate change impacts on plant pathogens, food security and paths forward. *Nat. Rev. Microbiol.* **2023**, *21*, 640–656. [CrossRef]
4. Ullah, I.; Mao, H.; Rasool, G.; Gao, H.; Javed, Q.; Sarwar, A.; Khan, M.I. Effect of Deficit Irrigation and Reduced N Fertilization on Plant Growth, Root Morphology and Water Use Efficiency of Tomato Grown in Soilless Culture. *Agronomy* **2021**, *11*, 228. [CrossRef]
5. Chauhdary, J.N.; Li, H.; Ragab, R.; Hussain, Z.; Anjum, S.A.; llxomovich, M.K. Modeling wheat growth to determine economic feasibility under deficit irrigation and nitrogen management strategies. *Agric. Water Manag.* **2025**, *319*, 109740. [CrossRef]
6. West, P.C.; Gerber, J.S.; Engstrom, P.M.; Mueller, N.D.; Brauman, K.A.; Carlson, K.M.; Cassidy, E.S.; Johnston, M.; MacDonald, G.K.; Ray, D.K.; et al. Leverage points for improving global food security and the environment. *Science* **2014**, *345*, 325–328. [CrossRef]
7. Mueller, N.D.; Gerber, J.S.; Johnston, M.; Ray, D.K.; Ramankutty, N.; Foley, J.A. Closing yield gaps through nutrient and water management. *Nature* **2012**, *490*, 254–257. [CrossRef]
8. Chauhdary, J.N.; Li, H.; Ragab, R.; Hussain, Z.; Akhlaq, M.; Lakhiar, I.A. Effects of water quality and nitrogen on wheat productivity: Experimental and modelling study using the SALTMED model. *Irrig. Drain.* **2025**, *74*, 688–702. [CrossRef]
9. Markwell, J.; Osterman, J.C.; Mitchell, J.L. Calibration of the Minolta SPAD-502 leaf chlorophyll meter. *Photosynth. Res.* **1995**, *46*, 467–472. [CrossRef]
10. Uddling, J.; Gelang-Alfredsson, J.; Piikki, K.; Pleijel, H. Evaluating the relationship between leaf chlorophyll concentration and SPAD-502 chlorophyll meter readings. *Photosynth. Res.* **2007**, *91*, 37–46. [CrossRef]
11. Li, M.; Li, J.; Wei, X.; Zhu, W. Early diagnosis and monitoring of nitrogen nutrition stress in tomato leaves using electrical impedance spectroscopy. *Int. J. Agric. Biol. Eng.* **2017**, *10*, 194–205.
12. Jócsák, I.; Végvári, G.; Vozáry, E. Electrical impedance measurement on plants: A review with some insights to other fields. *Theor. Exp. Plant Physiol.* **2019**, *31*, 359–375. [CrossRef]
13. Van Haeverbeke, M.; De Baets, B.; Stock, M. Plant impedance spectroscopy: A review of modeling approaches and applications. *Front. Plant Sci.* **2023**, *14*, 1187573. [CrossRef]
14. Basak, R.; Wahid, K.; Dinh, A. Determination of Leaf Nitrogen Concentrations Using Electrical Impedance Spectroscopy in Multiple Crops. *Remote Sens.* **2020**, *12*, 566. [CrossRef]
15. Zhang, C.; Su, Y.; Wu, Y.; Li, H.; Zhou, Y.; Xing, D. Comparison on the Nutrient Plunder Capacity of *Orychophragmus violaceus* and *Brassica napus* L. Based on Electrophysiological Information. *Horticulturae* **2021**, *7*, 206. [CrossRef]
16. Zhang, Q.; Xing, D.; Wu, Y.; Zhao, K.; Wang, J.; Mao, R. Effects of Low-Phosphorus Stress on Use of Leaf Intracellular Water and Nutrients, Photosynthesis, and Growth of *Brassica napus* L. *Horticulturae* **2024**, *10*, 821. [CrossRef]

17. Xing, D.; Chen, X.; Wu, Y.; Xu, X.; Chen, Q.; Li, L.; Zhang, C. Rapid prediction of the re-watering time point of *Orychophragmus violaceus* L. based on the online monitoring of electrophysiological indexes. *Sci. Hortic.* **2019**, *256*, 108642. [CrossRef]
18. Qin, X.; Xing, D.; Wu, Y.; Wang, W.; Li, M.; Solangi, K. Diurnal Variation in Transport and Use of Intracellular Leaf Water and Related Photosynthesis in Three Karst Plants. *Agronomy* **2022**, *12*, 2758. [CrossRef]
19. Gonzalez, I.J.D.; Najdenovska, E.; Dutoit, F.; Raileanu, L.E. Detecting stress caused by nitrogen deficit using deep learning techniques applied on plant electrophysiological data. *Sci. Rep.* **2023**, *13*, 9633. [CrossRef]
20. Sai, K.; Sood, N.; Saini, I. Classification of various nutrient deficiencies in tomato plants through electrophysiological signal decomposition and sample space reduction. *Plant Physiol. Biochem.* **2022**, *186*, 266–278. [CrossRef]
21. Tran, D.; Najdenovska, E.; Dutoit, F.; Plummer, C.; Wallbridge, N.; Mazza, M.; Camps, C.; Raileanu, L.E. Advanced assessment of nutrient deficiencies in greenhouse with electrophysiological signals. *Hortic. Environ. Biotechnol.* **2024**, *65*, 567–580. [CrossRef]
22. Kovács, F.; Juhos, K.; Odry, Á.; Ladányi, M.; Papdi, E.; Gyalai, I.M.; Simon, G.; Gergely, M.; Süli, Á.; Donyina, G.A.; et al. Early detection of nitrogen status in cucumber plants using bioimpedance spectroscopy. *Smart Agric. Technol.* **2025**, *12*, 101610. [CrossRef]
23. Armada-Moreira, A.; Dar, A.M.; Zhao, Z.; Cea, C.; Gelinas, J.; Berggren, M.; Costa, A.; Khodagholy, D.; Stavrinidou, E. Plant electrophysiology with conformable organic electronics: Deciphering the propagation of Venus flytrap action potentials. *Sci. Adv.* **2023**, *9*, eadh4443. [CrossRef]
24. Lee, G.; Hossain, O.; Jamalzadegan, S.; Liu, Y.; Wang, H.; Saville, A.C.; Shymanovich, T.; Paul, R.; Rotenberg, D.; Whitfield, A.E.; et al. Abaxial leaf surface-mounted multimodal wearable sensor for continuous plant physiology monitoring. *Sci. Adv.* **2023**, *9*, eade2232. [CrossRef]
25. Hurlbert, S.H. Pseudoreplication and the Design of Ecological Field Experiments. *Ecol. Monogr.* **1984**, *54*, 187–211. [CrossRef]
26. Poorter, H.; Fiorani, F.; Stitt, M.; Schurr, U.; Finck, A.; Gibon, Y.; Usadel, B.R.; Munns, R.; Atkin, O.K.; Tardieu, F.O.; et al. The art of growing plants for experimental purposes: A practical guide for the plant biologist. *Funct. Plant Biol.* **2012**, *39*, 821–838. [CrossRef]
27. Varma, S.; Simon, R. Bias in error estimation when using cross-validation for model selection. *BMC Bioinform.* **2006**, *7*, 91. [CrossRef]
28. Cawley, G.C.; Talbot, N.L.C. On Over-fitting in Model Selection and Subsequent Selection Bias in Performance Evaluation. *J. Mach. Learn. Res.* **2010**, *11*, 2079–2107.
29. Roberts, D.R.; Bahn, V.; Ciuti, S.; Boyce, M.S.; Elith, J.; Guillera-Arroita, G.; Hauenstein, S.; Lahoz-Monfort, J.J.; Schröder, B.; Thuiller, W.; et al. Cross-validation strategies for data with temporal, spatial, hierarchical, or phylogenetic structure. *Ecography* **2017**, *40*, 913–929. [CrossRef]
30. Zhang, C. Role of Pathogenic Organics of Sclerotinia in *Brassica napus* and *Orychophragmus violaceus* and Application of Electrophysiological Information in its Prediction and Control. Doctoral Dissertation, Jiangsu University, Zhenjiang, China, 2021.
31. Tan, X.; Wang, H.; Li, J.; Zhang, S.; Zheng, S.; Zhao, Z.; Zhang, B.; Wu, Y.; Zhao, C.; Li, S.; et al. Electrophysiological signatures decode herbivore-specific defense dynamics and elicitor-induced immune activation in rice. *Crop Health* **2025**, *3*, 19. [CrossRef]
32. Hoagland, D.R.; Arnon, D.I. *The Water-Culture Method for Growing Plants without Soil*; Circular 347; College of Agriculture, University of California: Berkeley, CA, USA, 1950.
33. Xiong, D.; Chen, J.; Yu, T.; Gao, W.; Ling, X.; Li, Y.; Peng, S.; Huang, J. SPAD-based leaf nitrogen estimation is impacted by environmental factors and crop leaf characteristics. *Sci. Rep.* **2015**, *5*, 13389. [CrossRef]
34. Fanourakis, D.; Makraki, T.; Tsaniklidis, G.; Ntatsi, G.; Körner, O. Technological innovations driving yield gains in greenhouse vegetables: Species-specific perspectives. *Sci. Hortic.* **2026**, *368*, 115180. [CrossRef]
35. Yu, R.; Wu, Y.; Xing, D. The Differential Response of Intracellular Water Metabolism Derived from Intrinsic Electrophysiological Information in *Morus alba* L. and *Broussonetia papyrifera* (L.) Vent. Subjected to Water Shortage. *Horticulturae* **2022**, *8*, 182. [CrossRef]
36. Tsaniklidis, G.; Makraki, T.; Papadimitriou, D.; Nikoloudakis, N.; Taheri-Garavand, A.; Fanourakis, D. Non-Destructive Estimation of Area and Greenness in Leaf and Seedling Scales: A Case Study in Cucumber. *Agronomy* **2025**, *15*, 2294. [CrossRef]
37. Field, C.A.; Welsh, A.H. Bootstrapping clustered data. *J. R. Stat. Soc. Ser. B (Stat. Methodol.)* **2007**, *69*, 369–390. [CrossRef]

Disclaimer/Publisher's Note: The statements, opinions and data contained in all publications are solely those of the individual author(s) and contributor(s) and not of MDPI and/or the editor(s). MDPI and/or the editor(s) disclaim responsibility for any injury to people or property resulting from any ideas, methods, instructions or products referred to in the content.